Graphene/Polyamide Laminates for Supercritical CO$_2$ and H$_2$S Barrier Applications: An Approach toward Permeation Shutdown

Thomas P. Raine, Oana M. Istrate, Barnaby E. King, Bernadette Craster,* Ian A. Kinloch, and Peter M. Budd*

Graphene is potentially the perfect barrier material, being impermeable even to the smallest gas molecules, but in practice it is difficult to achieve defect-free graphene layers at large scale. Here, exceptional barrier performance for laminates comprising graphene nanoplatelet (GNP) paper sandwiched between two discs of polyamide 11 (PA11) is demonstrated. Results are compared with sandwich structures incorporating melt-processed GNP/PA11 composites, and with chemical vapor deposition (CVD) monolayer graphene transferred onto PA11. PA11 is of interest as a polymer commonly utilized within the oil and gas industry for antiwear and barrier layers in flexible risers. Permeation studies were undertaken for a feed mixture of carbon dioxide (CO$_2$) with 1.48% hydrogen sulfide (H$_2$S) at a temperature of 60 °C and pressures up to 400 bar, providing the first data for the performance of graphene as a barrier to a supercritical fluid. Whereas a GNP/PA11 composite and a CVD graphene monolayer have little effect on permeability, compared to a pure PA11 control sample, a GNP/PA11 laminate reduces CO$_2$ permeability by more than an order of magnitude, and reduces H$_2$S permeability to an undetectable level.

One of the remarkable properties of graphene is its impermeability to gases, with perfect monolayer graphene being impervious to even helium.[1,2] Chemical vapor deposition (CVD) is an effective way of synthesizing large-area monolayer graphene; however, such graphene is typically defective.[3] Stacking of many CVD graphene layers improves the barrier performance of a system, by masking defects and grain boundaries with flawless regions.[4–8] This route, however, is time consuming, expensive, and inherently difficult to scale. Multilayered graphene nanoplatelets (GNPs) offer a cheap and potentially scalable alternative to CVD graphene coatings for use in barrier materials.[9,10] Wu and Drzal[9] created a GNP paper by filtration of a GNP suspension, and impregnated the porous structure with polyetherimide (PEId). The resulting GNP composite had an oxygen permeability that was 1.1% of that of the control PEId. Pierleoni et al.[10] also investigated filtered papers of GNPs and reported that even at graphene loadings as low as 0.4 wt%, a 74% depreciation in oxygen permeability could be achieved. An alternative route to improve the fluid barrier performance of thermoplastic polymers is through incorporation of GNPs via melt processing.[11–13] Gaska et al.[11] achieved improvements in barrier performance of low-density polyethylene (LDPE) to CO$_2$ and SF$_6$ of 65.5 and 80.5%, respectively, for LDPE loaded with 7.5 wt% GNP. Checchetto et al.[12] found 5 wt% GNPs reduced LDPE permeability to H$_2$, N$_2$, and CO$_2$ by ≈40%. Additionally, Honaker et al.[13] were able to reduce the permeability of high-density polyethylene (HDPE) by 73 and 74% for oxygen and hydrocarbon fuel vapor, respectively, at 15 wt% GNP loading. Low loadings of graphene and related materials can increase the permeability of polymers to gases, which is useful for separations.[14–16] Before the advent of graphene-based technology, clay had been used as a barrier additive. Adewole et al.[17] added organoclays to HDPE and investigated the permeation of CH$_4$ and CO$_2$ mixtures with varying compositions, in the temperature range of 30–70 °C and at pressures between 5 and 10 MPa. A maximum reduction in permeation compared to pure HDPE of 47% was achieved for 5 wt% nanoclay in HDPE at 50 °C and 10 MPa.

T. P. Raine, Prof. P. M. Budd
School of Chemistry
University of Manchester
Manchester M13 9PL, UK
E-mail: Peter.Budd@manchester.ac.uk
Dr. O. M. Istrate, Prof. I. A. Kinloch
School of Materials
University of Manchester
Manchester M13 9PL, UK
B. E. King, Dr. B. Craster
Materials Business Group
TWI Ltd.
Cambridge CB21 6AL, UK
E-mail: Bernadette.Craster@TWI.co.uk

The ORCID identification number(s) for the author(s) of this article can be found under https://doi.org/10.1002/admi.201800304.

To date, the literature has not considered the efficacy of graphene as a barrier material for high-pressure gases and supercritical fluids. One application in which high-pressure fluid permeability is important is in the oil and gas industry. Flexible risers transport crude mixtures from the seafloor to floating rigs, and are typically made up of many concentric layers of polymers and carbon steel.[18] Since the turn of the century, nearly two-thirds of the flexible pipes in use contain polyamide 11 (PA11) as an internal barrier pressure sheath.[19] Along with a range of hydrocarbons, crude usually contains water and highly corrosive "sour" fluids, including CO_2 and H_2S at high pressures and temperatures.[20] Upon permeating through the internal PA11 barrier layer, CO_2, H_2S, and water can corrode the crucial steel armor layers,[21] potentially leading to catastrophic failure. Dependent upon the well conditions, fluid temperatures within the flexible risers are typically below 100 °C, but pressures can exceed 100 MPa.[20] Herein, we present a route for the production of GNP/PA11 laminates and, for the first time, demonstrate their extraordinary barrier properties to supercritical fluids. We compare the GNP/PA11 laminates with GNP/PA11 nanocomposite sandwich structures and CVD graphene coated PA11, showing the efficacy of the GNP laminates.

Three ways of forming a graphene barrier within PA11 were investigated, as illustrated in **Figure 1**a and described in detail in the Supporting Information. Two different PA11 grades were used: BESVO extrusion grade pellets and BMNO injection molded plaques. First, GNP/PA11 laminates were prepared by compression molding GNP paper between two discs of BESVO PA11. Two different diameters of GNP paper were investigated: Laminate A was made up of 40 mm diameter GNP paper that provided complete coverage across the PA11 disks; Laminates B and C were made up of 35 mm diameter GNP paper and were sealed around the circumference by PA11.

Second, GNP/PA11 nanocomposites with a concentration of 1 wt% GNP were prepared by melt mixing on a twin-screw extruder. Then sandwich structures were prepared by compression molding melt-processed nanocomposite discs (0.5 mm thickness) between two discs of BESVO PA11. For comparison purposes, discs with melt-processed neat PA11 (0 wt%) were also prepared.

Third, CVD graphene coated BMNO PA11 plaque samples were prepared by cutting prestenciled plaques to the appropriate size.

The key parameter used to judge the efficacy of a barrier material is the permeability coefficient, P, which can be expressed as the product of a diffusion coefficient, D, and a solubility coefficient, S (Equation (1))[22]

$$P = DS \tag{1}$$

For a composite material, measured transport parameters are an average for the various phases present, but nevertheless provide a useful basis for comparison. Preliminary permeability measurements with 100% H_2S at 0.2 MPa demonstrated a large reduction in apparent H_2S permeability for GNP/PA11 laminates, compared to CVD graphene coated PA11 (see the Supporting
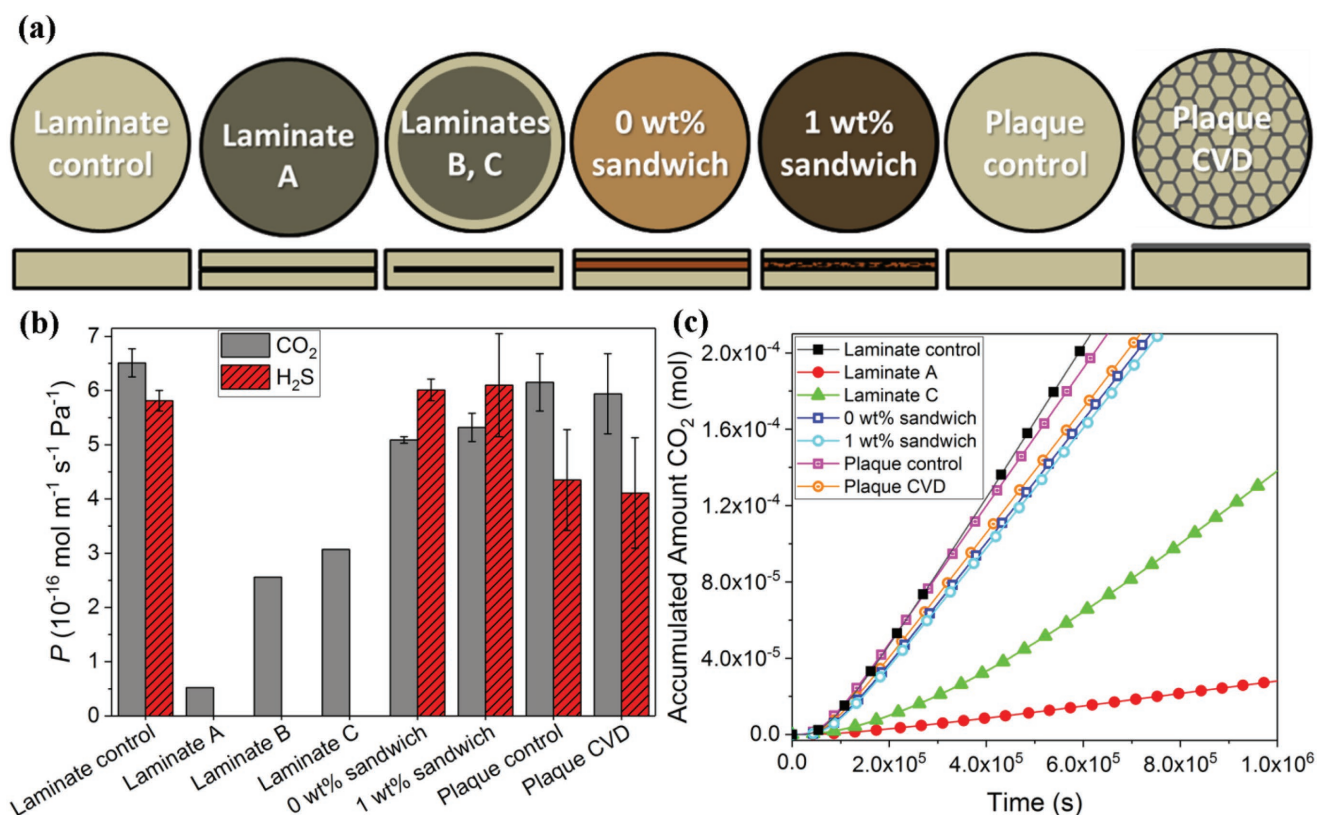
Figure 1. Permeation at 5 MPa and 60 °C for a feed gas mixture of CO_2 with 1.48% H_2S, for samples prepared by different methods. a) Schematic of sample appearance with cross-sectional structure; b) apparent CO_2 and H_2S permeability coefficients; c) representative plots of accumulated amount of CO_2 against time, from which P and D are determined.
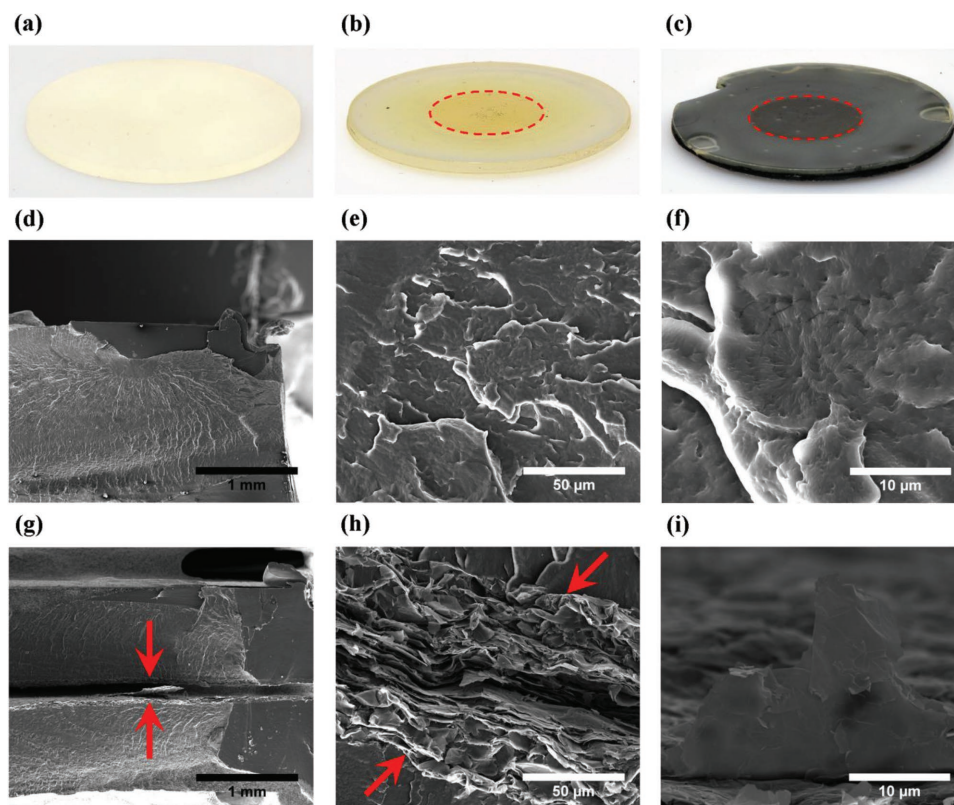
Figure 2. a) Unexposed control BESVO PA11 disk; b) exposed control BESVO PA11 control; c) exposed Laminate A; d–f) SEM images of cryogenically fractured BESVO PA11 control sample cross section following exposure, showing the polymer morphology. g–i) SEM images of cryogenically fractured Laminate A cross section showing polymer morphology and GNP layering. The red dotted ellipse in (b) and (c) highlights the region which was directly exposed to the fluid. The red arrows in (g) and (h) indicate the central GNP layer.

Information). Further experiments were conducted with a mixture of CO_2 with 1.48% H_2S at 60 °C for a series of pressures up to 40 MPa, monitoring both CO_2 and H_2S in the permeate.

Apparent permeability data at 5 MPa for the graphene-containing PA11 barrier materials, and control samples without graphene, are shown in Figure 1b. Error bars represent a single standard deviation from the mean of 2–6 measurements; results for Laminate A, Laminate B, and Laminate C are from single measurements. Errors for CO_2 are typically in the region of 5% and errors for H_2S are in the region of 10%. The laminate control was made from compression molded BESVO PA11 whereas the plaque control was injection molded BMNO PA11, and they differ in their permeability coefficients. Comparisons should be made to the appropriate control samples: laminate samples with laminate control; 1 wt% sandwich with 0 wt% sandwich; plaque CVD with plaque control. In Figure 1b, comparing the 0 and 1 wt% nanocomposite sandwich structures, it can be seen that there is no appreciable difference (within error) in permeability for CO_2 and H_2S at 5 MPa. The same appears to be true for plaque CVD when compared to the plaque control. The apparent poor performance of CVD graphene as a barrier material has been observed before.[6–8] We attribute this to large graphene free regions being present, an unavoidable result of the transfer process, as shown through Raman mapping (see the Supporting Information).[23,24]

In contrast to the nanocomposite sandwich and CVD graphene samples, the laminates show much reduced apparent

CO_2 permeability coefficients compared to the laminate control, and no detectable permeation of H_2S at 5 MPa. The CO_2 and H_2S data in Figure 1b demonstrate exceptional barrier performance for laminated GNP paper structures. Laminate A performed better than Laminates B and C. As Laminate A was not sealed around the edge, it is likely that at high pressure the GNPs had greater freedom to reorganize into a more compact barrier layer. Unlaminated, neat GNP paper had very high permeability and required compaction during compression molding to impart any barrier effect. The values in Figure 1b are apparent permeability coefficients for the composite structures. Calculated permeabilities of the GNP layers within the laminates are presented in the Supporting Information. Figure 1c shows representative plots of the accumulated amount of CO_2 over time. The laminate samples have markedly reduced gradients compared to the other samples displayed, which led to the low apparent permeability coefficients obtained.

Figure 2a shows a photograph of the semitransparent and colorless PA11 control before exposure. Figure 2b,c shows photographs of samples following exposure to the high-pressure CO_2 with 1.48% H_2S feed. The region directly exposed to the fluid is highlighted by a red dotted line on each sample. The large bubbles around the circumference of Laminate A were not directly exposed to the fluid, so should not affect the transport properties measured. The control PA11 yellows following exposure to H_2S, which we attribute to the evolution of
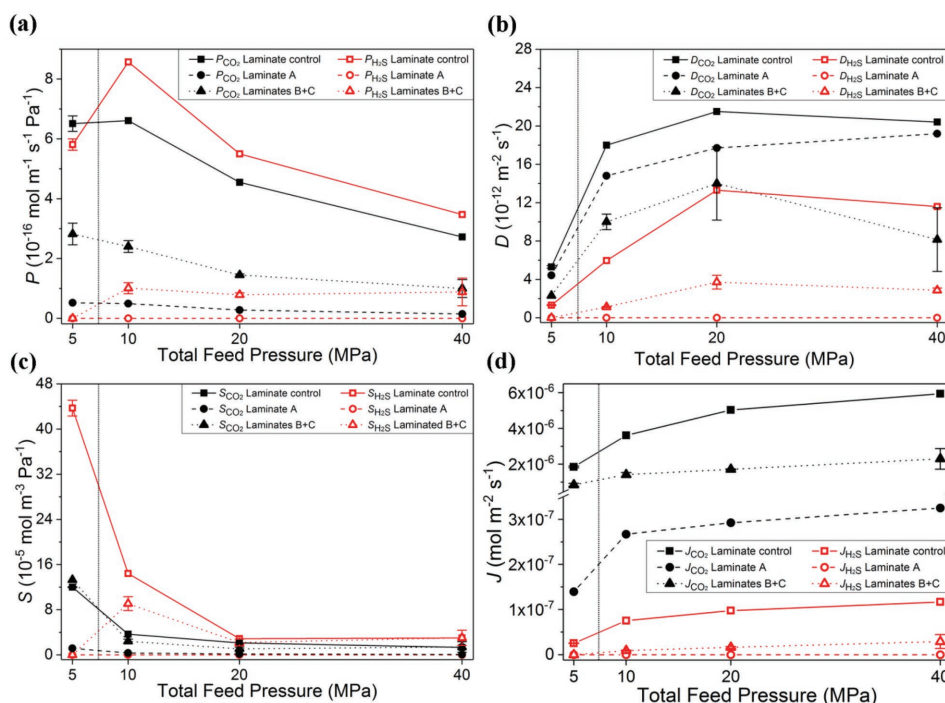
Figure 3. Dependence on total feed pressure of the apparent transport properties at 60 °C of CO_2 and H_2S through a pure PA11 laminate control and through GNP paper laminates (for Laminates B and C the values are averaged). The vertical line signifies the approximate location of the critical pressure for CO_2. a) Apparent permeability coefficient, P. b) Apparent diffusion coefficient, D. c) Apparent solubility coefficient, S. d) Flux, J.

elemental sulfur, confirmed through UV–vis spectroscopy (see the Supporting Information). We suggest that this effect is due to H_2S scrubbing at the amine end groups and amide bonds of the polymer, analogous to acid gas scrubbing with alkanolamines and polymeric amines.[25–27] It is worth noting that the yellowing is not only limited to the central exposed region and it would appear that lateral H_2S diffusion is extensive.

Figure 2d–i shows the secondary electron (SE) scanning electron microscopy (SEM) images of cryogenically fractured cross sections of the exposed Laminate control (Figure 2d–f) and Laminate A (Figure 2g–i). The macroscopic morphology of the polymer appears to be similar for both samples, as demonstrated in Figure 2d,g. Figure 2g shows the central graphene layer within the laminate structure (highlighted by red arrows), demonstrating the different physical structures of the control PA11 and the GNP paper laminate. Figure 2e,h shows the differences between the central regions of the two samples. As can be seen in Figure 2h, the graphene center (highlighted by red arrows) has a layered structure with preferential alignment perpendicular to the flow of permeating species. This is likely due to the vacuum filtration method employed to form the GNP paper as well as the high pressure compression molding used to form Laminate A. It is worth noting that Figure 2h was taken at the partially delaminated outer edge of the sample, as the two polymer surfaces at the center were completely delaminated during SEM sample preparation. The arrangement in Figure 2h is therefore somewhat expanded compared to the native arrangement of the GNPs following filtration, compression molding, and subsequent high-pressure testing. Figure 2f shows detailed morphology of the PA11 at the fracture surface. Figure 2i shows a large graphene flake protruding from the

GNP paper center in the delaminated region. The flake has a diameter of ≈25 μm, which is the quoted diameter of the supplied GNP flakes.[28]

For GNP/PA11 laminates, **Figure 3** shows the variation of apparent permeability, diffusion, and solubility coefficients and flux as functions of the total feed pressure, for pressures up to 40 MPa, at a temperature of 60 °C. The feed mixture is gaseous at 5 MPa.[29] CO_2 reaches a critical point at ≈7.4 MPa (marked by a vertical line in Figure 3); therefore, at 10 MPa and above, CO_2 is in the supercritical phase. It is assumed that the 1.48% H_2S is dissolved in the CO_2 phase.[29] For Laminates B and C, the apparent transport coefficients are averaged and the error bars signify a single standard deviation of the two samples. As can be seen in Figure 3a, there was a striking reduction in both apparent CO_2 and H_2S permeability in the laminate samples, compared to the pure PA11 laminate control. For Laminate A, the apparent permeability of CO_2 was consistently reduced by over an order of magnitude, and the H_2S permeability was undetectable over all pressures. For Laminates B and C, the apparent CO_2 permeability was reduced by half and the H_2S permeability was undetectable (below GC detection limit) at 5 MPa. At 10 MPa and above, the apparent H_2S permeability of Laminates B and C was reduced by up to 90% compared to the control. The difference between the apparent permeability of Laminate A and Laminates B and C appear to be related to differences in the sample preparation (Laminates B and C had a PA11 seal around the edge, as indicated in Figure 1a). The extraordinary performance of Laminate A is likely to be due to the well-ordered GNP paper structure affording a highly tortuous pathway for the diffusion of molecules. The apparent total barrier to H_2S may be due to reducing the permeation to

below the detection limit of the GC, which is over an order of magnitude less than the H_2S measured for the control. Additionally, we suggest that H_2S can be complexed by the PA11, so ultralow levels of H_2S breaking through the graphene center are likely to be captured within the polymer, as elemental sulfur (see the Supporting Information).

Figure 3a suggests that the gas selectivity of the PA11 control favors CO_2 permeation in the gas phase, but switches to favor H_2S permeation once the CO_2 becomes supercritical. Interestingly, the apparent diffusion coefficients in Figure 3b, for the control PA11, indicate that the CO_2 diffusion rate remained higher than the H_2S diffusion rate. This suggests that CO_2 behaves as a smaller and harder penetrant than H_2S and diffuses quickly through the membrane. The complementary effect can be seen in Figure 3c, as the apparent solubility coefficients of H_2S in PA11 appeared far higher than those of CO_2. CO_2 is likely to interact strongly with PA11 and may behave as a Lewis acid by accepting electrons from carbonyl oxygen in amide bonds.[30] Indeed, CO_2 has been known to lower the melting point of polyamides, by interrupting hydrogen bonding between adjacent polymer chains—an effect utilized in supercritical CO_2 processing of nylons.[31] Nitrogen-containing materials do, however, tend to have a high selectivity for binding H_2S.[32,33] Vaughn and Koros[34] found that the sorption coefficients of H_2S were consistently higher than those of CO_2 in polyamide–imide systems. In CH_4 with CO_2 and H_2S mixed gas tests, H_2S was found to plasticize the polyamide–imide whereas CO_2 did not.[34] The complexation of H_2S to amide bonds or amine end groups, and their subsequent reaction, may also be the cause of the dramatic yellowing observed in the PA11 samples. More work is required to establish the mechanism. Figure 3d shows that as the pressure increased, the flux across the membrane increased. The flux, however, does not take into account the increasing pressure or the membrane thickness.

In conclusion, the apparent permeability of gaseous and supercritical CO_2 and H_2S mixtures through PA11, GNP/PA11 laminates, GNP/PA11 nanocomposite sandwich structures, and CVD graphene coated PA11, has been investigated. GNP/PA11 laminates have superior barrier performance compared to other GNP-containing and graphene-containing barrier materials tested. A GNP paper laminate can reduce apparent CO_2 permeability by over an order of magnitude, and reduce H_2S permeability to an undetectable level, for all pressures up to 40 MPa. Future work will explore further the effects of GNP papers of various thicknesses and investigate alternative methods of processing GNPs into barrier films.

Experimental Section

Materials: GNP powder was sourced from XG Sciences Inc., USA. xGnP Grade M with 25 µm platelet size was chosen. All PA11 grades were sourced from Arkema Inc., France. BESVO A FDA approved grade was chosen for melt-processing and compression molding, and was supplied in pellet form. BMNO injection molded plaques were also provided. CVD graphene was grown and applied to prestenciled BMNO PA11 plaques by 2-DTech, UK. N-Methyl-2-pyrrolidone was supplied by Sigma-Aldrich Company Ltd., UK. All materials were used as received unless otherwise stated.

Sample Preparation: See the Supporting Information.

Characterization: SEM was carried out on Au/Pd coated cryogenically fractured samples at 10 kV on a FEI Quanta 250 FEG SEM.

Gas permeation: Permeation testing was carried out on a purpose built high-pressure rig at TWI Ltd., Cambridge, UK. The samples were placed in a high-pressure test cell. For CVD graphene coated plaques and GNP laminates, a protective PA11 gasket was placed on the surface. The cell was sealed tight. The sealed cells were placed in an oven at 60 °C and the feed gas was pumped to pressure. The feed gas was premixed dry CO_2 with 1.48% H_2S supplied by CK Gas Ltd., UK. The laminates' experimental profile ran to a steady state at 60 °C, at the following gauge pressures: 5, 10, 20, and 40 MPa. The test ran for ≈7 weeks in total. The CVD graphene samples and GNP/PA11 composite sandwich structure samples ran to the steady state at 60 °C and at gauge pressures of 5 and 10 MPa. The mathematical background of the method may be found in the Supporting Information.

Supporting Information

Supporting Information is available from the Wiley Online Library or from the author.

Conflict of Interest

The authors declare no conflict of interest.

Keywords

[1] J. S. Bunch, S. S. Verbridge, J. S. Alden, A. M. van der Zande, J. M. Parpia, H. G. Craighead, P. L. McEuen, *Nano Lett.* **2008**, *8*, 2458.

[2] O. Leenaerts, B. Partoens, F. M. Peeters, *Appl. Phys. Lett.* **2008**, *93*, 193107.

[3] T. H. Seo, S. Lee, H. Cho, S. Chandramohan, E.-K. Suh, H. S. Lee, S. K. Bae, S. M. Kim, M. Park, J. K. Lee, M. J. Kim, *Sci. Rep.* **2016**, *6*, 24143.

[4] H.-K. Seo, M.-H. Park, Y.-H. Kim, S.-J. Kwon, S.-H. Jeong, T.-W. Lee, *ACS Appl. Mater. Interfaces* **2016**, *8*, 14725.

**ADVANCED
SCIENCE NEWS**

www.advancedsciencenews.com

**ADVANCED
MATERIALS
INTERFACES**

www.advmatinterfaces.de

[5] S. Seethamraju, S. Kumar, K. B. B, G. Madras, S. Raghavan, P. C. Ramamurthy, *ACS Nano* **2016**, *10*, 6501.

[6] K. Choi, S. Nam, Y. Lee, M. Lee, J. Jang, S. J. Kim, Y. J. Jeong, H. Kim, S. Bae, J.-B. Yoo, S. M. Cho, J.-B. Choi, H. K. Chung, J.-H. Ahn, C. E. Park, B. H. Hong, *ACS Nano* **2015**, *9*, 5818.

[7] C. Wirtz, N. C. Berner, G. S. Duesberg, *Adv. Mater. Interfaces* **2015**, *2*, 1500082.

[8] M. O. Paraense, T. H. R. da Cunha, A. S. Ferlauto, K. C. de Souza Figueiredo, *J. Appl. Polym. Sci.* **2017**, *134*, 45521.

[9] H. Wu, L. T. Drzal, *Carbon* **2012**, *50*, 1135.

[10] D. Pierleoni, Z. Y. Xia, M. Christian, S. Ligi, M. Minelli, V. Morandi, F. Doghieri, V. Palermo, *Carbon* **2016**, *96*, 503.

[11] K. Gaska, R. Kádár, A. Rybak, A. Siwek, S. Gubanski, *Polymers* **2017**, *9*, 294.

[12] R. Checchetto, A. Miotello, L. Nicolais, G. Carotenuto, *J. Membr. Sci.* **2014**, *463*, 196.

[13] K. Honaker, F. Vautard, L. T. Drzal, *Mater. Sci. Eng., B* **2017**, *216*, 23.

[14] K. J. Berean, J. Z. Ou, M. Nour, M. R. Field, M. M. Y. A. Alsaif, Y. Wang, R. Ramanathan, V. Bansal, S. Kentish, C. M. Doherty, A. J. Hill, C. McSweeney, R. B. Kaner, K. Kalantar-zadeh, *J. Phys. Chem. C* **2015**, *119*, 13700.

[15] B. M. Yoo, J. E. Shin, H. D. Lee, H. B. Park, *Curr. Opin. Chem. Eng.* **2017**, *16*, 39.

[16] K. Althumayri, W. J. Harrison, Y. Shin, J. M. Gardiner, C. Casiraghi, P. M. Budd, P. Bernardo, G. Clarizia, J. C. Jansen, *Philos. Trans. R. Soc., A* **2016**, *374*, 2060.

[17] J. K. Adewole, L. Jensen, U. A. Al-Mubaiyedh, N. von Solms, I. A. Hussein, *J. Polym. Res.* **2012**, *19*, 9814.

[18] Y. Shen, J. Zhao, Z. Tan, T. Sheldrake, in *ASME 2012 31st Int. Conf. Ocean, Offshore and Arctic Engineering*, OMAE, Rio de Janerio, Brazil **2012**.

[19] S. Groves, in *20th Int. Conf. Offshore Mechanics and Arctic Engineering*, OMAE, Rio de Janeiro, Brazil **2001**.

[20] F. A. Dawans, J. A. Jarrin, T. O. Lefevre, M. A. Pelisson, in *18th Annual Offshore Technology Conf.*, Offshore Technology Conference, Houston, TX **1986**.

[21] B. Flaconnèche, J. Martin, M. H. Klopffer, *Oil Gas Sci. Technol.* **2001**, *56*, 245.

[22] S. Matteucci, Y. Yampolskii, B. D. Freeman, I. Pinnau, in *Materials Science of Membranes for Gas and Vapor Separation* (Eds: Y. Yampolskii, I. Pinnau, B. D. Freeman), Wiley, Chichester, England **2006**, pp. 1–47.

[23] G. J. M. Fechine, I. Martin-Fernandez, G. Yiapanis, R. Bentini, E. S. Kulkarni, R. V Bof de Oliveira, X. Hu, I. Yarovsky, A. H. Castro Neto, B. Özyilmaz, *Carbon* **2015**, *83*, 224.

[24] C. J. An, S. J. Kim, H. O. Choi, D. W. Kim, S. W. Jang, M. L. Jin, J.-M. Park, J. K. Choi, H.-T. Jung, *J. Mater. Chem. A* **2014**, *2*, 20474.

[25] B. P. Mandal, S. S. Bandyopadhyay, *Chem. Eng. Sci.* **2005**, *60*, 6438.

[26] A. L. Kohl, R. B. Nielsen, *Gas Purification*, Gulf Publishing Company, Houston, TX **1985**, pp. 41–186.

[27] Y. Bai, T. G. J. Jones, B. Craster, A. Hammami, T. Yakimoski, *US20090277*, **2009**.

[28] XG Sciences Inc., "xGnP Graphene Nanoplatelets Technical Data Sheet: Grade M Characteristics," http://xgsciences.com/wp-content/uploads/2012/10/10-15-13_xGnP-M_Data-Sheet.pdf (accessed: 2013).

[29] D. P. Sobocinski, F. Kurata, *AIChE J.* **1959**, *5*, 545.

[30] S. G. Kazarian, M. F. Vincent, F. V. Bright, C. L. Liotta, C. A. Eckert, *J. Am. Chem. Soc.* **1996**, *118*, 1729.

[31] J. D. Martinache, J. R. Royer, S. Siripurapu, F. E. Hénon, J. Genzer, S. A. Khan, R. G. Carbonell, *Ind. Eng. Chem. Res.* **2001**, *40*, 5570.

[32] H. R. Godini, D. Mowla, *Chem. Eng. Res. Des.* **2008**, *86*, 401.

[33] A. Haghtalab, A. Izadi, *Fluid Phase Equilib.* **2014**, *375*, 181.

[34] J. Vaughn, W. J. Koros, *Macromolecules* **2012**, *45*, 7036.

1800304 (6 of 6)